Monthly Notices
of the
ROYAL ASTRONOMICAL SOCIETY

Mon. Not. R. Astron. Soc. **400,** 406–421 (2009) doi:10.1111/j.1365-2966.2009.15495.x

Precision astrometry of a sample of speckle binaries and multiples with the adaptive optics facilities at the Hale and Keck II telescopes

K. G. Hełminiak,[1⋆] M. Konacki,[1,2] S. R. Kulkarni[3] and J. Eisner[4]

[1]*Nicolaus Copernicus Astronomical Center, Department of Astrophysics, ul. Rabiańska 8 , 87-100 Toruń, Poland*
[2]*Astronomical Observatory, A. Mickiewicz University, Sloneczna 36, 60-286 Poznan, Poland*
[3]*Division of Physics, Mathematics and Astronomy, California Institute of Technology, Pasadena, CA 91125, USA*
[4]*Steward Observatory, University of Arizona, Tucson, AZ 85721, USA*

Accepted 2009 July 28. Received 2009 July 27; in original form 2009 March 16

ABSTRACT

Using the adaptive optics facilities at the 200-in Hale and 10-m Keck II, we observed in the near-infrared a sample of 12 binary and multiple stars and one open cluster. We used the near diffraction limited images of these systems to measure the relative separations and position angles between their components. In this paper, we investigate and correct for the influence of the differential chromatic refraction and chip distortions on our relative astrometric measurements. Over one night, we achieve an astrometric precision typically well below 1 mas and occasionally as small as 40 μas. Such a precision is in principle sufficient to astrometrically detect planetary mass objects around the components of nearby binary and multiple stars. Since we have not had sufficiently large data sets for the observed sample of stars to detect planets, we provide the limits to planetary mass objects based on the obtained astrometric precision.

Key words: instrumentation: adaptive optics – astrometry – binaries: visual – planetary systems.

1 INTRODUCTION

In the field of exoplanets, astrometry has not had too many triumphs to date. Of over 350 known planets or planetary candidates, only one has been discovered astrometrically (Pravdo & Shaklan 2009). The astrometric results presented by Han, Black & Gatewood (2001) are disputable and the true masses of only a few planets were calculated more reliably by combining the radial velocities (RV) and astrometry from the *Hubble Space Telescope* and the ground-based observations (Benedict et al. 2002, 2006). Nevertheless, astrometry may just turn out to be the most promising planet detection method in the future. Astrometric space missions, like Space Interferometry Mission (SIM) (Unwin et al. 2008) or *Gaia* (Perryman 2005), and a few ground-based interferometric surveys are ongoing (e.g. Lane & Muterspaugh 2004) or are in preparation (e.g. on the VLTI; Eisenhauer et al. 2008; Launhardt et al. 2008; Sahlman et al. 2008). In particular, ground-based interferometers seem to be already well suited to detect planets by providing microarcsecond (μas) astrometric precision (e.g. Muterspaugh et al. 2005) for bright nearby binary stars.

The milliarcsecond (mas) or better precision can be achieved by imaging with the adaptive optics (AO) systems. This was already demonstrated for two binaries, HD 19063 and HD 19994, observed with the VLT (Neuhäuser et al. 2006; Röll, Seifhart & Neuhäuser 2008) and a globular cluster M5 observed with the Hale telescope (Cameron, Britton & Kulkarni 2009). Such a precision can be reached by means of relative astrometry over a small field of view (Cameron et al. 2009). To this end, one needs to have at least one reference object not too far from a science object. For this reason, visual and speckle binaries become a natural target for such measurements. Incidentally, the subject of the existence of exoplanets in binary and multiple stars has become of significant interest (e.g. Raghavan et al. 2006; Eggenberger et al. 2007; Muterspaugh et al. 2007; Mugrauer & Neuhäuser 2009). It is now accepted that the detection or lack of planets in star systems will provide additional constraints to our models of planet formation (e.g. Holman & Weigert 1999; Nelson 2000; Lissauer et al. 2004).

In this paper, we present our observations of a sample of 12 binary and multiple stars and one open cluster obtained in 2002 with the AO facilities at the Hale and Keck II telescopes over the period of 7 months. We investigate the influence of several systematic effects that have an impact on the relative astrometry and demonstrate that by correcting them one can achieve a sub-mas precision. Finally, we provide the limits to planetary mass objects around components of our target stars derived from the obtained astrometric precision.

2 OBSERVATIONS

2.1 Instrumentation

The main instrument in our project was the 200-inch Hale Telescope at the Palomar Observatory. We used PHARO (*the Palomar High Angular Resolution Observer*; Hayward et al. 2001) camera with PALAO (*the PALomar Adaptive Optics*) system. PHARO uses

⋆E-mail:xysiek@ncac.torun.pl

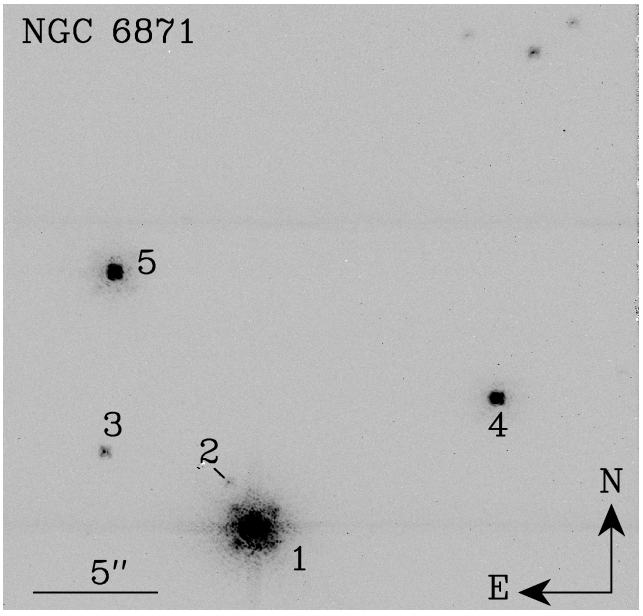

Figure 1. A field in NGC 6871 centred on $\alpha = 20^{\rm h}05^{\rm m}57^{\rm s}$, $\delta = 35^\circ47'25''$ as seen on 2002 June 23. Positions of only five labelled stars were measured. Other three (top of the image) are not seen in images from other nights. FOV is 25 × 25 arcsec. North is up, east is left.

a mosaic of four 512 × 512 HgCdTe HAWAII detectors for observations between 1 and 2.5 μm (Hayward et al. 2001). PALAO is an AO system mounted at the Cassegrain focus of the telescope. It employs a Shack–Hartman wavefront sensor and a Xinetics Inc. 349/241 active-element deformable mirror. PALAO's detailed description can be found online.[1]

With Hale/PALAO we obtained about 30 000 images of our targets. The data were collected over seven nights between 2002 April and November. We used an imaging mode with 39.91 and mostly 25.10 mas pixel^{-1} scale and *K*, *K'*, *Ks* broad, as well as Brγ and Fe II narrow band filters. We also used a 1 per cent transmission neutral density filter ND-1 for decreasing a flux from very bright stars. Dithering was carried out by shifting the observed position by ∼2 as.

We also had one clear night at the 10-m Keck II telescope. Using its AO system and NIRC2 (*the Near InfraRed Camera 2*) we obtained data for three targets and the total of about 600 images. NIRC2 is a mosaic of four 512 × 512 InSb Aladdin-3 detectors. For the observations we used 9.942 and 39.686 mas pixel^{-1} scale and the *J*, *K'* and *K*-cont (narrow-band) filters. Dithering was done using field rotation.

2.2 Objects

From all the attempted objects we selected nine binaries/multiples from the Hale data set and three multiples from the Keck II one. These are: GJ 195, GJ 352, GJ 458, GJ 507, GJ 661, GJ 767, GJ 860, GJ 873 and GJ 9071 for the Hale, and GJ 300,[2] GJ 569 and 56 Per for the Keck II. All systems are shown in Fig. 2. We also selected a field in the open cluster NGC 6871 (the Hale data set) centred around $\alpha = 20^{\rm h}05^{\rm m}57^{\rm s}$, $\delta = 35^\circ47'25''$ as a reference field to study the systematic effects (Fig. 1).

[1] http://ao.jpl.nasa.gov/Palao/PalaoIndex.html
[2] Two fainter stars seen close to GJ 300 and GJ 873 are actually field stars.

The selection criterion we adopted for the Hale sample was mainly the high number of individual images and also the number of nights during which a given object was observed. The exception is GJ 352. It was selected to study a precision of astrometry for a low number of single images. For the Keck II observations, it was mostly important to check how good the AO correction was and how many unsaturated stars were in an image (see Fig. 2). Due to saturation we were able to measure the relative positions only for the double secondary components of the Keck targets. The last two issues were caused by the varying weather conditions and hence highly variable AO correction. The final numbers of individual images per night used in the analysis for a particular object, after rejection of useless data, are given in Table 1.

Our objects are mostly M-type dwarfs located less than 20 pc from the Sun. In a few cases (e.g. GJ 195), not only a binary but also other stars were captured in an image. Their relative positions were also measured. For the open cluster, the astrometry was performed only for five stars but other objects can be seen in images as well. For all the stars which are catalogued the basic information is given in Table 2. Column 'No.' refers to a number/label in an image. The higher is the number assigned, the fainter the star is.

3 POSITION CALCULATIONS

The images were first reduced with standard IRAF tasks for data reduction. Subsequently, given the number of exposures, the relative positions of the stars were computed with our own software in an automated manner as follows. (1) The shifts from image to image (due to the dithering) were measured by cross-correlating the template image (usually the first image) with all the subsequent exposures, and the approximate positions of stars in a given image were calculated with an accuracy of ±3 pixel (∼75 mas for most of the Hale's sample). (2) Based upon these positions, the centroids were calculated. (3) Based upon the centroids, the following two-dimensional elliptical Gaussian function was fitted to the cores of the images of stars:

$$G(x, y) = B + A \exp\left[-\frac{[(x - x_0)\cos\theta - (y - y_0)\sin\theta]^2}{2\sigma_x^2} - \frac{[(x - x_0)\sin\theta + (y - y_0)\cos\theta]^2}{2\sigma_y^2}\right], \quad (1)$$

where B is a background level, A is the amplitude of a Gaussian, (x_0, y_0) is a position of the star, σ_x, σ_y are the corresponding widths and θ is a tilt of the Gaussian.

We have decided to use such an approach because it offers a simple and robust way of modelling the cores of stars' images. One could envision using an empirical point spread function (PSF) as a model for the images of stars. This is, however, challenging due to the fact that in a single image we typically have only two stars. Hence, our knowledge about the actual empirical PSF for a given frame is limited. Additionally, since the PSF's shape varies, it is not practical to use several subsequent exposures as a reference for an averaged empirical. This is demonstrated in Fig. 3 for a series of five frames of GJ 661 taken on June 23 and spanning 15.5 min, for which an average empirical PSF is calculated using a 9 pixel aperture and subtracted from the images of stars. As can be seen a fitting of the Gaussian performs better. The details of this procedure are also given in Table 3.

The results of the Gaussian fitting were used to compute the relative separations and the position angles of pairs of stars. The NIRC2 data were corrected for the field rotation used for dithering. Let us note that we did not use any weighting scheme for individual

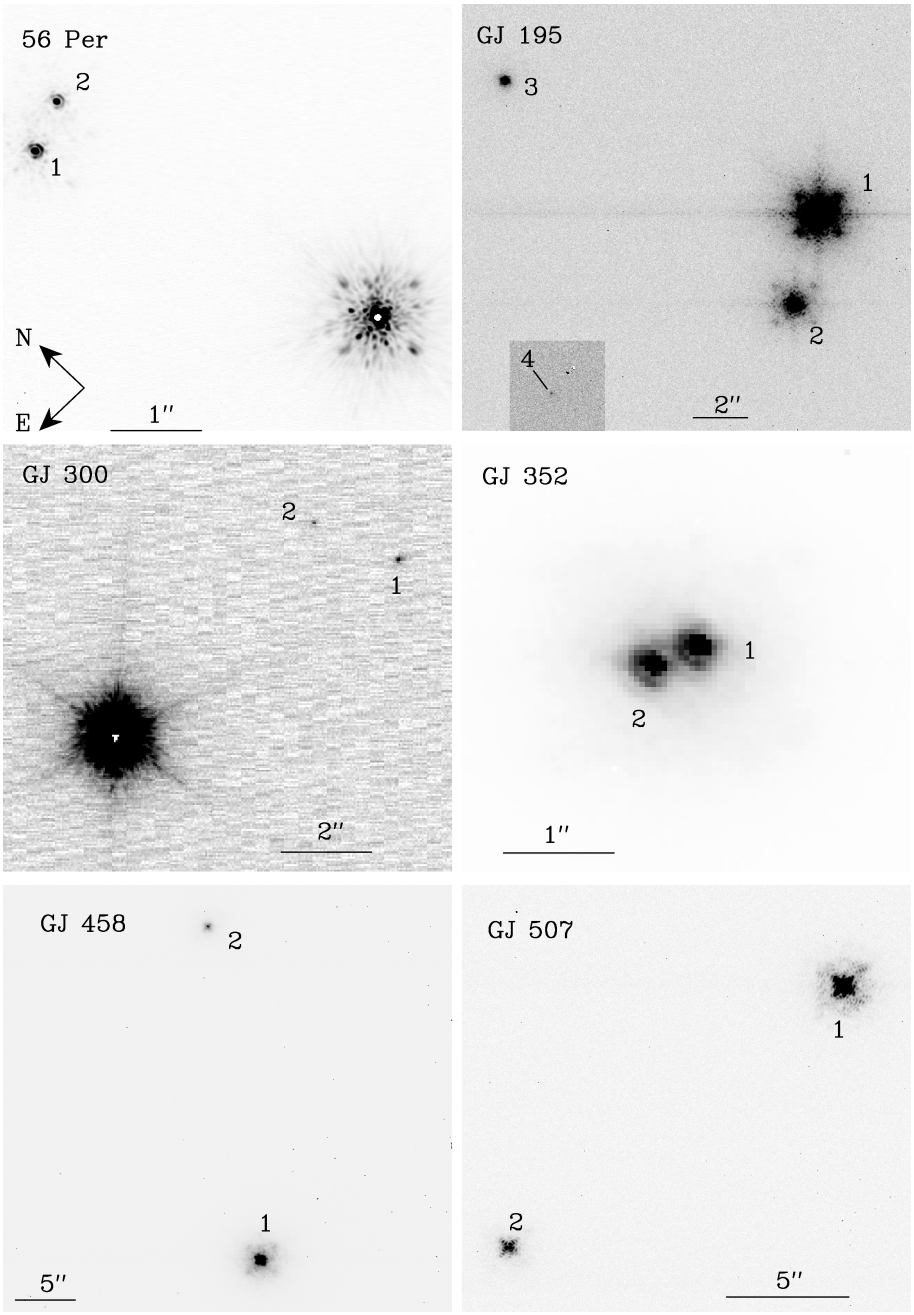

Figure 2. Images for all observed systems and labels of investigated stars. North is up and east is left except for 56 Per where north is up-left (rotation by 44.°7, as shown). FOV size varies, separations are given in Table 6. The saturated cores of the primary components of 56 Per and GJ 300 are clearly seen. GJ 569 A is also saturated but this is not seen in the adopted scale.

images as it was done by Cameron et al. (2009). A significant improvement in the astrometric precision after using an optimal weighting is seen when the number of reference stars exceeds five (see fig. 2 in Cameron et al. 2009) which is never the case in our work targeting binary stars and aimed at investigating the astrometric precision in the case of only one reference star.

4 SYSTEMATIC EFFECTS

4.1 Adaptive optics correction and field of view

The main factor allowing us to obtain precise astrometric measurements is obviously the AO. Its performance will influence the final astrometric precision as can be seen in the case of GJ 352 ($\rho \simeq 350$ mas) observed during challenging weather conditions. From all 75 images of GJ 352 taken, only the first 10 were properly corrected (the Airy pattern visible) and only in 53 images components were resolved and could be analysed. For these 53 images the centroids were calculated. Subsequent Gaussian fitting was possible only for 34 images for which the fitting procedure converged. The centroids and the outcome of Gaussian fitting are in agreement for the first 10 (Fig. 4).

Another factor having an impact on the astrometric precision is the field of view and the corresponding PSF sampling which was especially important for the Keck II data. The images were taken in two pixel scales (field sizes) – 9.942 mas pixel^{-1}

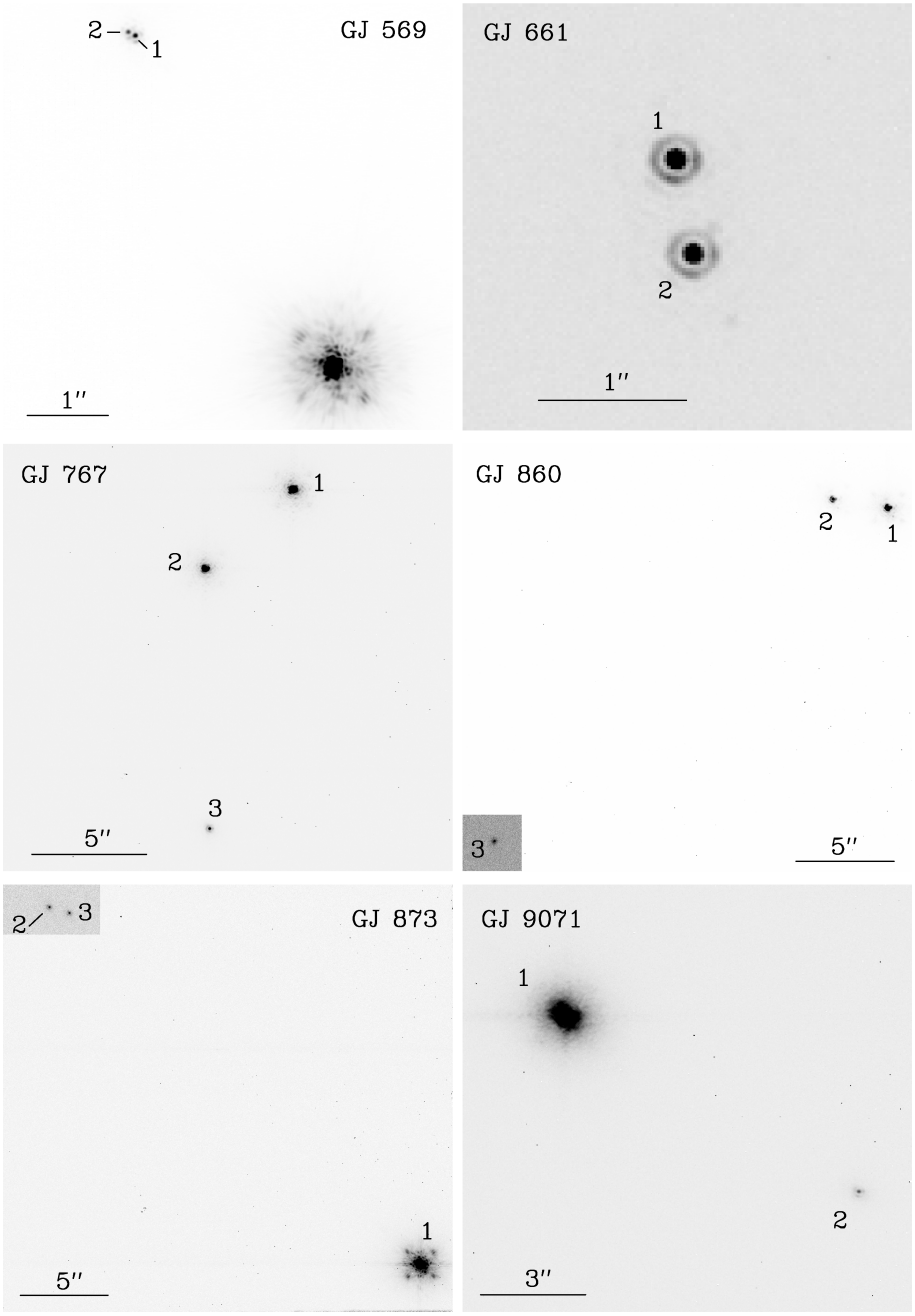

Figure 2 – *continued*

(10 × 10 arcsec^2 field, narrow) and 39.686 mas pixel^{-1} (40 × 40 arcsec^2 field, wide) and in various field rotator angles –45.°7, 0.°7 and −44.°3. For this telescope the diffraction-limited size of a star's image in the near infrared corresponds to about 1.4 pixel in the wide field. For faint stars, it means that most of their light is collected in one pixel which makes the PSF undersampled and the Gaussian fitting difficult. This issue, however, can be at least partially overcome by a sub-pixel dithering. For the purpose of this paper, we used only the frames taken with the 'narrow' field.

4.2 Atmospheric refraction

The atmospheric differential refraction (ADR) creates a shift of star's image. It is highly dependent on the zenith angle and wavelength. Formulae for computing ADR effect are given, for example, by Roe (2002) where the angle R, which is the difference between the real and observed zenithal distance, is given by

$$R \equiv z_{\rm t} - z_a \simeq 206265 \left(\frac{n^2-1}{2n^2}\right) \tan z_{\rm t} \ [\text{arcsec}], \quad (2)$$

where $z_{\rm t}$ is the true zenithal distance, z_a is the observed zenithal distance and n is the refraction index, dependent on the wavelength λ and weather conditions:

$$n(\lambda, p, T, p_w) = 1 + \left[64.328 + \frac{29498.1}{146-\lambda^{-2}} + \frac{255.4}{41-\lambda^{-2}}\right] \frac{pT_{\rm s}}{p_{\rm s}T} 10^{-6} - 43.49 \left[1 - \frac{0.007956}{\lambda^2}\right] \frac{p_w}{p_{\rm s}} 10^{-6}, \quad (3)$$

Table 1. Number of images of a particular object per night.

Night/tel.	56 Per	GJ 195	GJ 300	GJ 352	GJ 458
Mar. 04/K	58	–	58	–	–
Apr. 23/H	–	–	–	53	975
Jun. 23/H	–	–	–	–	1060
Jun. 24/H	–	–	–	–	685
Aug. 21/H	–	300	–	–	–
Aug. 22/H	–	582	–	–	–
Nov. 13 /H	–	949	–	–	–
Night/tel.	GJ 507	GJ 569	GJ 661	GJ 767	GJ 860
Mar. 04/K	–	29	–	–	–
Apr. 23/H	949	–	656	–	–
Jun. 23/H	1012	–	454	–	189
Jun. 24/H	520	–	800	–	1166
Jun. 26/H	–	–	1250	–	–
Aug. 21/H	–	–	750	569	600
Aug. 22/H	–	–	636	746	507
Nov. 13/H	–	–	–	745	584
Night/tel.	GJ 873	GJ 873B	GJ 9071		NGC 6871
Jun. 23/H	225	251	–		510
Jun. 24/H	510	497	–		1010
Aug. 21/H	200	200	750		1083
Aug. 22/H	200	200	513		2131
Nov. 13/H	300	–	1246		624

A faint, third component of the GJ 860 system was not always in the field of view (due to the dithering). Separate columns for GJ 873 and GJ 873B are to distinguish between the images of the full triple system and the double secondary only. 'K' stands for Keck II and 'H' for the Hale telescope.

where λ is given in μm, p, T and p_w are the pressure [hPa], temperature [K] and partial pressure of water vapour, respectively. Symbols with the index s refer to the canonical values of air pressure (1013.25 hPa) and temperature (288.15 K). The angle R is much smaller in IR than in visible.

ADR also affects relative astrometric measurements. Since two objects are seen at different zenithal distances z_1 and z_2, the corrections R_1 and R_2 are also different. The component of the separation, vector parallel to the direction to the zenith, increases after ADR correction by $\Delta R = |R_2 - R_1|$. This quantity changes with weather conditions (air pressure and temperature). As we have demonstrated (Hełminiak 2009), the magnitude of this change is often higher than an achievable astrometric precision even for relatively compact systems. Clearly, ADR's influence must be corrected and the weather conditions should be well known. This conclusion is in contrary to that by Neuhäuser et al. (2006), who claim that the refraction is, in general, insignificant, thanks to the use of a narrow bandpass filter (chromatic refraction). As the ADR is dependent on the zenithal distance, it may be significant even for a monochromatic light. So, the real reason why ADR is negligible in case of Neuhäuser et al. (2006) is likely the geometry of their binary. Nevertheless, it is true that using wide-band filters makes ADR harder to calculate due to its chromatic character and, for example, stars' different colours (Hełminiak 2009).

Unfortunately, we did not collect any weather readings during our observing runs, so we had to use the canonical values of temperature and pressure, and assumed 50 per cent humidity. For the Keck observations we assumed two times smaller pressure and the temperature of 0°C. This means that the real uncertainties of measured separations and position angles are higher than the precisions given in Table 6. To correct for ADR, we used the semifull approach as described by Hełminiak (2009).

In order to estimate the maximum error due to ADR, we took the largest possible separation in our sample – 30.8 as for GJ 873 1-2 (from Table 6). We assumed that the difference in the zenithal angles equals the separation, and the binary is seen 30° above the horizon. In such an improbable case, the maximum contribution to the error budget coming from the temperature is 4 mas (if the real temperature were $T = 230$ K and pressure $p = 1013.25$ hPa) and the fraction coming from the air pressure is smaller than 8 mas (for $p = 613$ hPa and $T = 230$ K). One should add that the bigger the part coming from the temperature, the smaller is the contribution from the pressure. So we may conclude that in this improbable case 8, mas is the maximum error and in most (if not all) of our real observations the uncertainty caused by the weather conditions is smaller than several mas. In the case of binaries observed with Keck II, the maximum error should be much smaller because the separations (and z differences) are smaller and other, more probable weather conditions were assumed. The maximum uncertainty scales linearly with air pressure and almost linearly with separation (maximum z difference) and temperature. In Section 5.1 we estimate, in yet another way, the observed rms of our astrometric measurements.

4.3 Chip geometry and orientation

Detectors are not perfectly rectangular, flat and perpendicular to the light path. At the astrometric precision necessary to detect planets (well below 1 mas), one has to know how the camera's detector is distorted or how the pixel scale and the detector's orientation change from epoch to epoch. For instruments mounted in the Cassegrain focus, as is the case for PHARO, the distortion changes with the telescope's position due to gravity. This effect is not present or negligible in the case of NIRC2 which is located in a Nasmyth platform. The astrometric calibration and distortion models are available for both cameras. The calibration for PHARO is more complicated and includes not only the geometry and orientation of the detector itself but also the influence of telescope's position and tilt of the chip relative to the light path. This is described by Metchev (2006).[3] The distortion of the NIRC2 camera was investigated during its pre-ship testing and is described by Thompson, Egani & Sawicki (2001).[4]

The calibration we carried out included deriving the average plate-scale of the chip and the position of the north direction with respect to the Cassegrain ring (CR). The nominal values are 25.10 mas pixel^{-1} for the narrow, 39.91 mas pixel^{-1} for the wide field pixel scale and 335.°8 for CR (Hayward et al. 2001). As it was shown by Metchev & Hillenbrand (2004), the real values are different from the nominal one and usually change from epoch to epoch. As a base for our calibration, we adopted the measurements from 2002 June 23 by Metchev & Hillenbrand (2004) which are: 25.168 ± 0.034 mas pixel^{-1} and $334.^{\circ}043 \pm 0.^{\circ}099$. We chose four stars in NGC 6871, marked in Fig. 1 as 1–4 which we believe to be members of the cluster (their positions with respect to the star No. 5 changed in a similar way), and using their relative positions we have recalculated the average pixel scale in the narrow field by assuming that their astrometric motion is not detectable. First of all, for every night and every six possible pairs, we calculated a preliminary pixel scale and the north direction, incorporating the uncertainties from Metchev & Hillenbrand (2004). Later, we averaged the results for every single night. We checked if for two or more consecutive nights the pixel scale changed, and if it did not, we averaged the

[3] See http://www.astro.ucla.edu/∼metchev/ao.html

[4] See http://alamoana.keck.hawaii.edu/inst/nirc2/preship_testing.pdf

Table 2. Basic information on our targets.

Star	No.	Sp. type	Magn.	(Band)	π (mas)	Comment[a]	Telescope	Ref.
56 Per B	1+2	???	8.7	(*V*)	24.00 (.91)	Double	Keck II	1,2
GJ 195 A	1	M1	10.16	(*V*)	72.0(.4)	–	Hale	3,4
GJ 195 B	2	M5	13.7	(*V*)	72.0(.4)	–	Hale	3,4
AG+45 517	3	???	11	(*V*)	???	Field	Hale	4
GJ 300 B	1+2	K7III?	8.39	(*J*)	125.60(.97)[b]	Double, field	Keck II	5,6
GJ 352 A	1	M4	10.07	(*V*)	94.95(4.31)	–	Hale	1,7
GJ 352 B	2	M4	10.08	(*V*)	94.95(4.31)	–	Hale	1,7
GJ 458 A	1	M0	9.86	(*V*)	65.29(1.47)	–	Hale	1,8
GJ 458 B	2	M3	13.33	(*V*)	65.29(1.47)	–	Hale	1,8
GJ 507 A	1	M0.5	9.52	(*V*)	75.96(3.31)	–	Hale	1
GJ 507 B	2	M3	12.09	(*V*)	75.96(3.31)	–	Hale	1
GJ 569 Ba	1	M8.5V	11.14	(*J*)	101.91(1.67)	Double(?)[c]	Keck II	1,9,10,11
GJ 569 Bb	2	M9V	11.65	(*J*)	101.91(1.67)	–	Keck II	1,9,11
GJ 661 A	1	M3	10.0	(*V*)	158.17(3.26)	–	Hale	1,7
GJ 661 B	2	M4	10.3	(*V*)	158.17(3.26)	–	Hale	1,7
GJ 767 A	1	M1	10.28	(*V*)	74.90(2.93)	–	Hale	1,8
GJ 767 B	2	M2	11.10	(*V*)	74.90(2.93)	–	Hale	1,8
GJ 860 A	1	M3	9.59	(*V*)	249.53(3.03)	Variable	Hale	1,12
GJ 860 B	2	M4	10.30	(*V*)	249.53(3.03)	Flare	Hale	1,12
CCDM 22281...H[d]	3	???	13.8	(*V*)	???	Field	Hale	13
GJ 873 A	1	M3.5e	10.09	(*V*)	198.07(2.05)	Flare	Hale	1
GJ 873 B	2+3	G	10.66	(*V*)	198.07(2.05)	Double, field	Hale	1,14
GJ 9071 A	1	K7	10.2	(*V*)	72(4)	–	Hale	1,8,13
GJ 9071 B	2	M0	14	(*B*)	72(4)	–	Hale	1,13

[a]If 'double', magnitude refers to a total magnitude of both components and spectral type is 'averaged'. If 'field', the star is not gravitationally tied with brighter components.
[b]Parallax is for GJ 300, not the two investigated stars.
[c]Simon, Bender & Prato (2006) suggested that GJ 569 Ba may be a binary with similar brightness components.
[d]CCDM 22281...H = CCDM J22281+5741H – a part of a multi-stellar system which includes also GJ 860.
Ref.: (1) The *Hipparcos* Catalogue (Perryman et al. 1997); (2) Barstow et al. (2001); (3) Jenkins (1952); (4) The *PPM North* Catalogue (Roeser & Bastian 1988); (5) Simons, Henry & Kirkpatrick (1996); (6) Henry et al. (2006); (7) Al-Shukri et al. (1996); (8) Reid et al. (2004); (9) Lane & Muterspaugh (2004); (10) Simon et al. (2006); (11) Cutri et al. (2003); (12) Law, Hodgkin & McKay (2008); (13) *CCDM - Catalog of Components of Double & Multiple stars* (Dommanget & Nys 2002); (14) Oppenheimer et al. (2001).

result over the number of nights. This procedure allowed us to improve our pixel scale's uncertainties with respect to those given by Metchev & Hillenbrand (2004) who used only one pair while we used up to 18 (six pairs, observed during three nights). An adequate procedure was carried out for the CR orientation angle.

For three nights of 2002 August and November, we obtained the value of 25.156 ± 0.010 mas pixel^{-1} which is in poor agreement with the previous value, but then the difference in separations of the stars was clearly seen. We also recalculated new pixel scale for June 24 and obtained 25.171 ± 0.021 mas pixel^{-1} which shows that there was actually no scale change during one night. We also assumed the same plate-scale for the night of June 26. The cluster NGC 6871 was not observed in 2002 April but the results for GJ 458 suggest that the pixel scale and orientation were the same as in June. We assumed that the orbital period of GJ 458 is long enough that no orbital motion can be seen after 62 days and the separation remains constant. Comparing this system with GJ 195, which is closer to the Sun and has a few times smaller angular separation, we may conclude that the period is much longer than 338 years (orbital period of GJ 195; Heintz 1974), probably close to 3200 years. We see only a small (however clear) motion in GJ 195, and we should expect at least a 10 times smaller movement in GJ 458 which would be below the detection. Thus, for 2002 April we used the same pixel scale as for June 23 with its relatively high uncertainty.

This binary was also observed in the wide field mode on April 23 at the beginning of the night. By combining the measurements from the wide and narrow fields, we obtained 40.00 ± 0.02 mas pixel^{-1} as a pixel scale for the wide field and noticed no change in the CR angle. Between June and November, we noticed two changes of the CR orientation. The values of CR for August and November were $334\overset{\circ}{.}072 \pm 0\overset{\circ}{.}011$ and $334\overset{\circ}{.}723 \pm 0\overset{\circ}{.}015$, respectively. The recalculated value for June 24 and 26 was $334\overset{\circ}{.}039 \pm 0\overset{\circ}{.}018$. We should also note that the position angles were computed from Δx and Δy counted in pixels along the chip's axes, so the bigger the separation, the smaller is the uncertainty in θ.

Values of the derived plate-scale and north positions are summarized in Table 4. For the stars in the open cluster NGC 6871, we show the average values of separations together with their rms' (Table 5, Fig. 5). The average values are calculated from five epochs corrected for the new pixel scales. Such a calibration is not perfect, and these plate-scale and north direction values are subject to possible systematic errors, for example, due to a limited knowledge of the weather conditions.

Examples of the distortion and the results of employing its model can be seen in Fig. 6. We show the uncorrected and corrected measurements of separation $(\Delta x, \Delta y)$ for two stars in the NGC 6871 field. The distortion is clearly seen in the x-axis (the top-left panel). It is worth noting that for PHARO the distortion is much bigger in x than in y, but in the y-axis the random scatter is about 50 per cent

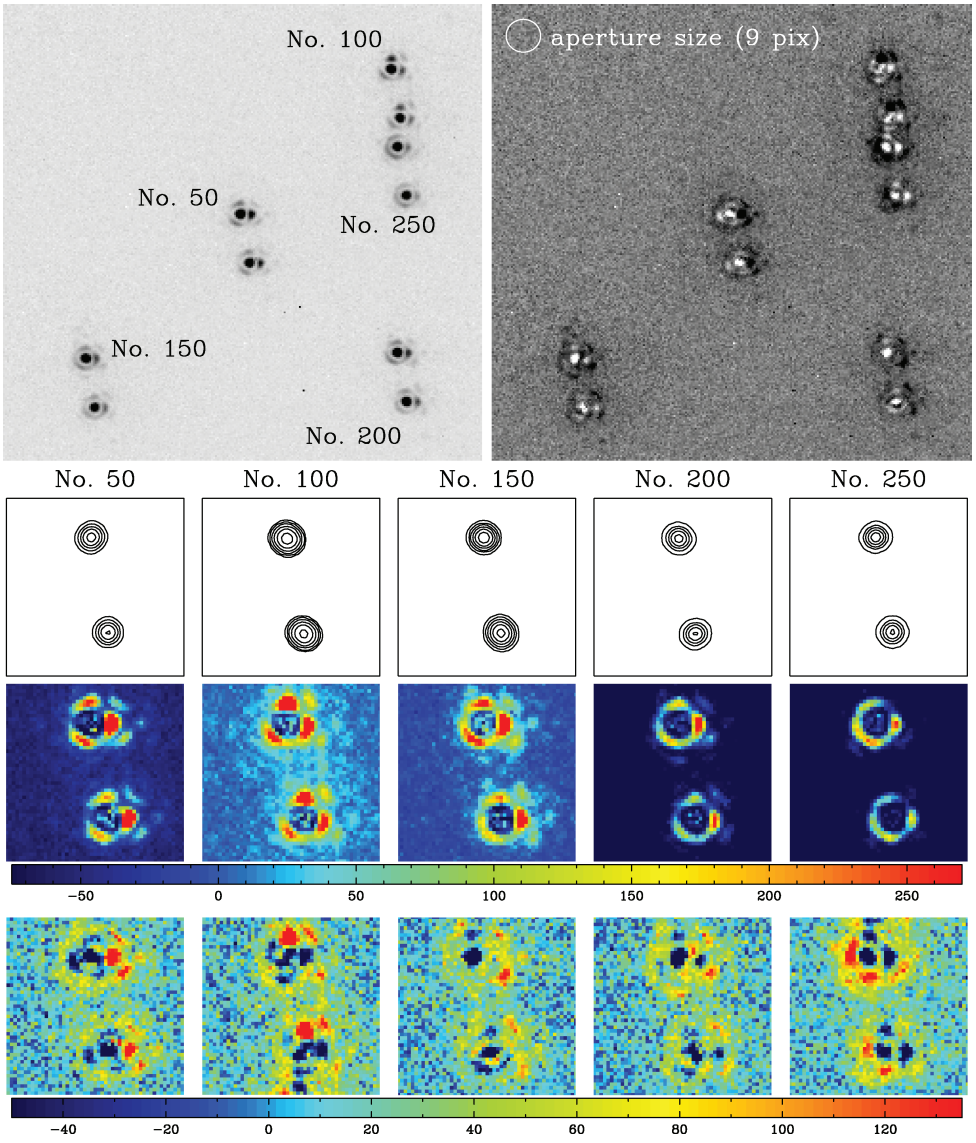

Figure 3. Top left: a combined image of GJ 661 from five exposures taken on June 23. The corresponding frame numbers are next to each image of the binary. Top right: a residual image after a subtraction of an empirical PSF (computed with DAOPHOT; Stetson 1987). The size of the fitting aperture (9 pixel in radius) is shown as a white circle. Upper middle: a 15 × 15 pixel zooms on the contour plots of the fitted Gaussian functions at the positions of respective stars. Contour levels vary. Gaussians clearly show significant variations of their shape. Lower middle: the same zooms on the residuals after the subtraction of the Gaussian functions. Changes of the first Airy ring can be seen. Colour scale is the same in every sub-panel. Bottom: the same zooms on the residuals after a subtraction of an empirical PSF. A clear leftover in the PSF core is evident. Colour scale is the same in every sub-panel.

bigger. The histograms demonstrate that after the correction, we are able to obtain a Gaussian statistics (the middle panels), and the Allan variance (AV) shows no obvious signs of systematic errors (the bottom panels).

The real average plate-scales of NIRC2 were found to be in agreement with the nominal values (Metchev & Hillenbrand 2004) but the *y*-axis was rotated by 1.°24 clockwise from north (Metchev et al. 2005). Unfortunately, due to a small number of useful images in our data set, we were not able to perform proper tests and our own calibrations. Hopefully, the location of the camera on the Nasmyth platform grants its stability. In particular, the results for 56 Per and GJ 569 B where three different field rotator positions were used demonstrates that the precision of the field rotator of NIRC2 is better than 0.°1 during one night.

5 ASTROMETRY

The astrometric measurements are presented in Table 6, where for each pair of stars and epoch (MJD) the separation $\rho\,[mas]$ and the position angle θ [in degree] are given. The 1σ errors were calculated using the Gaussian statistic of Δx and Δy. The plate-scale uncertainty is included into the separation error, but not into $\Delta\theta$ for Hale observations. It is because we wanted to show how small changes can be noticed between two nights where the same chip orientation is present (see GJ 860 1-2 in August – MJD = 52509 and 52510). CR orientation uncertainties are about one order of magnitude bigger, so they would dominate the θ error budget. The uncertainty in θ for GJ 300 is also underestimated because this system was observed with only one position of the field rotator of

Table 3. Parameters of an elliptical Gaussian function used to model the images of stars in the frames for GJ 661 (Fig. 3). An average value of a residual after a Gaussian and an empirical PSF subtraction are given together with its uncertainties in the last four columns. Analyzed frames are numbered as in Fig. 3.

Star frame/ID	A (counts)	σ_x (pixel)	σ_y (pixel)	x_0 (pixel)	y_0 [pixel]	B (counts)	θ (°)	Av. resid. (G)	σ	Av. resid. (PSF)	σ
No. 50/1	2846.443	1.505	1.432	543.897	615.032	13.231	130	17.59	18.16	−111.73	13.57
No. 50/2	2203.045	1.437	1.429	548.635	588.264	48.128	91	3.74	11.38	−101.62	10.73
No. 100/1	2711.196	1.399	1.499	622.879	694.661	−0.042	122	4.88	11.46	−39.33	5.68
No. 100/2	2125.978	1.378	1.512	627.583	667.851	−0.300	125	−3.95	14.32	−85.35	7.45
No. 150/1	2629.679	1.478	1.407	626.141	538.949	35.679	16	11.13	11.38	−130.78	10.17
No. 150/2	1953.843	1.636	1.527	630.955	512.050	−17.370	65	15.58	17.12	−116.19	17.75
No. 200/1	2391.502	1.395	1.488	462.866	535.715	59.381	115	3.06	10.35	−140.15	8.43
No. 200/2	1928.833	1.363	1.469	467.544	508.818	51.934	65	8.88	13.26	−75.02	7.67
No. 250/1	2344.759	1.436	1.349	626.177	652.063	81.791	165	2.47	7.87	−112.96	9.03
No. 250/2	1722.767	1.441	1.450	630.861	625.335	50.023	87	0.83	6.09	−67.74	7.36

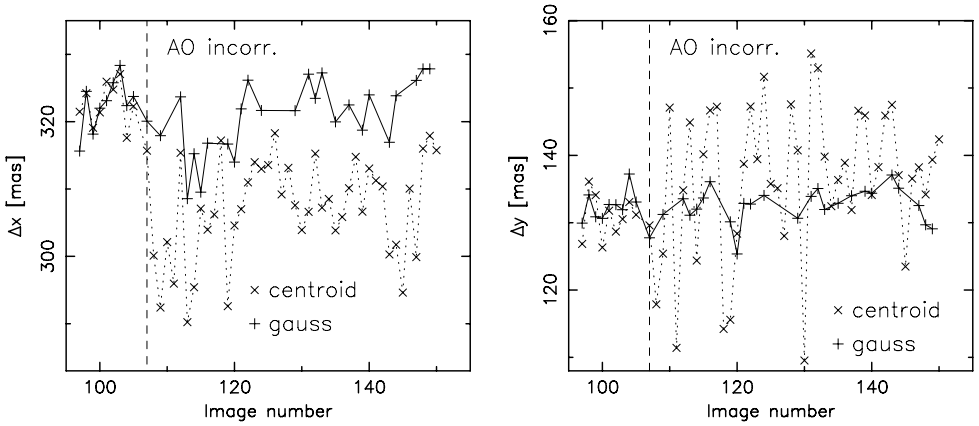

Figure 4. Impact of AO correction on relative position measurements in case of GJ 352. After image No. 107 (dashed line) AO works improperly.

Table 4. Average pixel scales and north orientations for Hale telescope.

Night	Scale (mas pixel^{-1})	North (○)
Apr. 23 (narrow)	25.168 (34)	334.043 (99)
Apr. 23 (wide)	40.00 (2)	334.043 (99)
Jun. 23	25.168 (34)	334.043 (99)
Jun. 24	25.171 (21)	334.039 (18)
Jun. 26	25.171 (21)	334.039 (18)
Aug. 21	25.156 (10)	334.072 (11)
Aug. 22	25.156 (10)	334.072 (11)
Nov. 13	25.156 (10)	334.723 (15)

Table 5. The average separations between the stars 1 to 4 in the NGC 6871 open cluster.

Pair	ρ (mas)	rms
NGC 6871 1–2	2171.719	0.604
1–3	6906.003	0.533
1–4	11303.461	1.023
2–3	5257.245	0.302
2–4	11463.147	1.194
3–4	16144.625	1.019

NIRC2. This is, however, not the case for 56 Per and GJ 569 B where different values of the field rotator were used for dithering. Hence, the resulting formal error of the position angle, presumably, more realistically reflects the accuracy of this AO system. For systems observed more than once, the orbital, parallactic and proper motion can be seen. Even for the long-period binary GJ 195 ($P \simeq 338$ yr; Heintz 1974), there is a clear signature of the orbital motion. Also a closer inspection of GJ 873 reveals a motion of the double secondary system (see Fig. 8). GJ 873 B is probably a real binary but at a different distance from the Sun than GJ 873 A (parallactic motion is present).

For five of our binaries(GJ 195, GJ 352, GJ 569 B, GJ 661 and GJ 860), the orbital solutions are known and can be found in the *Washington Double Star Catalog* (WDS).[5] The corresponding orbital elements are presented in Table 7. The quality of the orbit is represented by the parameter q – the smaller the value, the more accurate isthe orbital solution. In all the five cases the orbital solutions are not perfect, but only for GJ 195 the elements are poor due to a long period of the binary.

[5] Sixth Catalog of Orbits of Visual Binary Stars http://ad.usno.navy.mil/wds/orb6/orb6frames.html

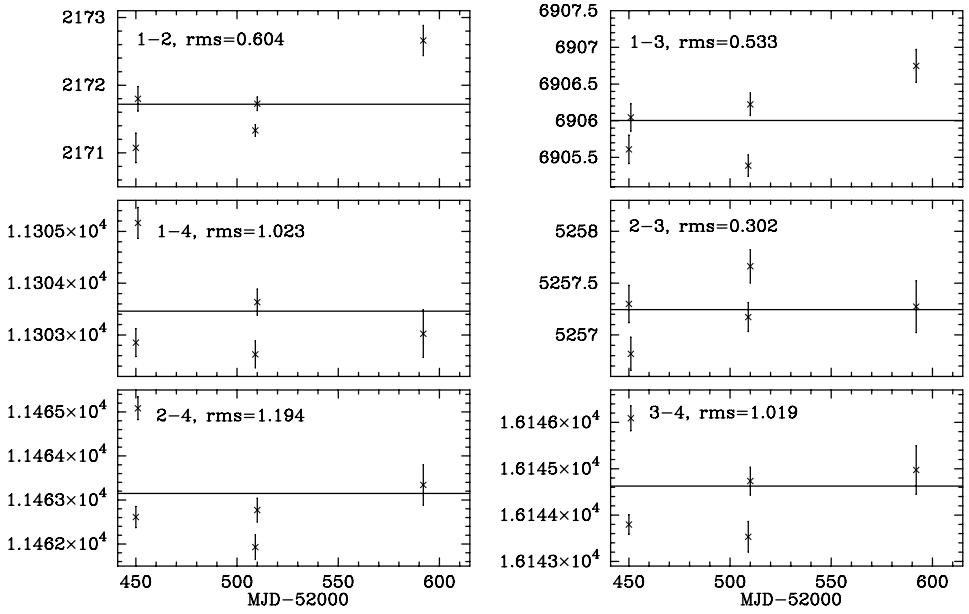

Figure 5. Separations of stars from the open cluster NGC 6871. The average value is plotted as a solid line and the corresponding *rms* in mas is shown.

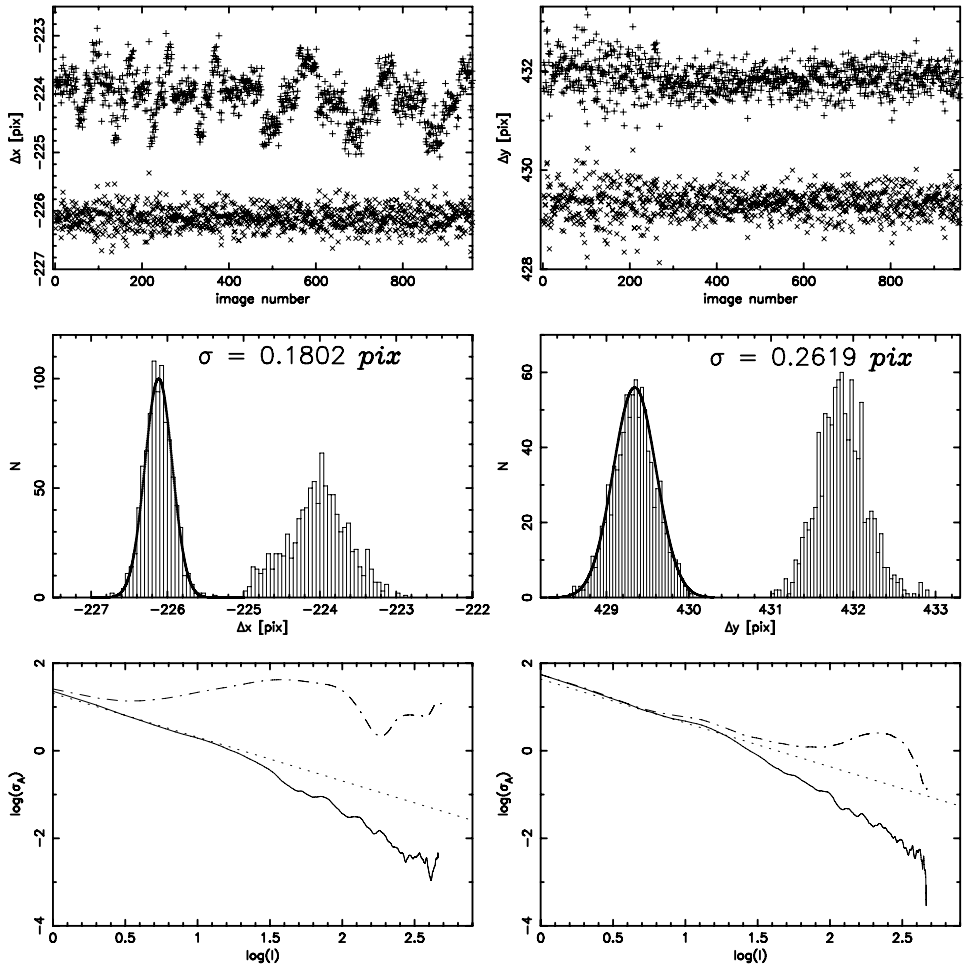

Figure 6. An example of the distortion and its correction for two stars in NGC 6871 cluster. Left-hand panels refer to X (α) component, right ones to Y (δ). Top panels: the measurements before (+) and after ($\times$, shifted) the distortion correction. Middle panels: the histograms of the measurements (bin width of 0.05 pixel) with a Gaussian fitted to the corrected measurements (left). Bottom panels: the AV of the uncorrected (dot–dashed) and corrected (solid) measurements and an infinitely long, white-noise signal with σ given in the middle panel (dotted line).

Table 6. Separations and position angles of investigated stars.

Pair	ρ (mas)	±	θ [°]	±	MJD	Pair	ρ [*mas*]	±	θ [°]	±	MJD
56 Per B						*GJ 767*					
1–2	626.31	0.32	291.733	0.039	52337	1–2	5276.64	0.17	135.4224	0.0014	52509
							5277.21	0.12	135.4129	0.0009	52510
GJ 195							5284.86	0.09	135.4630	0.0006	52592
1–2	3612.79	0.31	167.3130	0.0012	52509	1–3	16016.88	0.52	168.9361	0.0004	52509
	3613.02	0.23	167.3020	0.0009	52510		16017.73	0.28	168.9188	0.0002	52510
	3612.18	0.12	167.4167	0.0004	52592		15840.08	0.39	169.1386	0.0003	52592
1–3	12830.54	0.50	67.7436	0.0017	52509	2–3	11977.08	0.43	183.01454	0.00005	52509
	12831.67	0.44	67.7327	0.0018	52510		11977.06	0.22	182.99594	0.00002	52510
	12869.51	0.24	67.4695	0.0009	52592		11811.14	0.35	183.50265	0.00007	52592
1–4	12151.22	0.54	126.6784	0.0020	52509						
	12150.86	0.47	126.6756	0.0017	52510	*GJ 860*					
	12125.38	0.23	126.3902	0.0008	52592	1–2	2875.849	0.078	84.0520	0.0014	52450
2–3	13895.74	0.43	52.8881	0.0013	52509		2875.365	0.048	84.0420	0.0006	52451
	13896.73	0.46	52.8783	0.0016	52510		2858.542	0.061	83.2373	0.0010	52509
	13954.70	0.24	52.6982	0.0008	52592		2858.621	0.061	83.2063	0.0009	52510
2–4	9699.14	0.51	112.6419	0.0024	52509		2834.493	0.087	82.0401	0.0014	52592
	9698.21	0.47	112.6382	0.0022	52510	1–3	26525.54	0.73	133.9775	0.0012	52450
	9694.63	0.21	112.2336	0.0011	52592		26528.41	0.41	133.9754	0.0007	52451
3–4	12303.86	0.50	189.9677	0.0034	52509		26748.78	0.94	133.5531	0.0016	52509
	12305.32	0.60	189.9642	0.0004	52510		26755.53	1.37	133.5333	0.0025	52510
	12310.07	0.24	189.9467	0.0002	52592		26851.07	1.34	132.4185	0.0019	52592
						2–3	24771.78	0.75	139.0745	0.0012	52450
GJ 300 B							24775.50	0.42	139.0711	0.0007	52451
1–2	2035.74	0.12	66.6688	0.0018	52337		25020.13	0.91	138.5973	0.0015	52509
							25028.25	1.19	138.5767	0.0021	52510
GJ 352							25139.60	1.33	137.4029	0.0019	52592
1–2	346.21	1.11	113.6970	0.12	52389						
						GJ 873					
GJ 458						1–2	30155.85	0.57	47.0269	0.0009	52450
1–2	14723.58	0.40	10.55272	0.00024	52389		30158.79	1.07	47.0469	0.0016	52451
	14720.19	0.28	10.56016	0.00016	52450		30328.74	0.73	47.2967	0.0012	52509
	14723.27	0.36	10.55398	0.00021	52451		30334.65	0.60	47.3068	0.0009	52510
							30784.76	1.12	47.4235	0.0015	52592
GJ 507						1–3	29089.44	0.58	45.8990	0.0009	52450
1–2	17747.73	0.45	131.0180	0.0012	52389		29093.40	0.85	45.9219	0.0013	52451
	17757.84	0.33	131.0927	0.0006	52450		29260.32	0.76	46.1888	0.0012	52509
	17756.96	0.66	131.0845	0.0013	52451		29265.43	0.61	46.1990	0.0009	52510
							29717.16	1.03	46.3402	0.0014	52592
GJ 569 B						2–3	1215.619	0.067	255.1128	0.0034	52450
1–2	98.14	0.11	61.506	0.050	52337		1216.078	0.266	255.1578	0.0170	52451
							1214.913	0.085	255.0884	0.0044	52509
GJ 661							1215.301	0.100	255.0963	0.0048	52510
1–2	724.611	0.079	195.3279	0.0015	52389		1214.012	0.347	255.0787	0.0170	52592
	685.264	0.170	192.2382	0.0023	52450						
	685.065	0.044	192.1392	0.0007	52451	*GJ 9071*					
	683.084	0.038	192.0158	0.0006	52454	1–2	9971.76	0.20	239.5226	0.0009	52509
	643.316	0.058	188.7846	0.0006	52509		9972.00	0.26	239.5376	0.0012	52510
	642.957	0.041	188.7072	0.0004	52510		9924.03	0.24	240.0697	0.0011	52592

Table 7. Orbital elements of five of our binaries for which orbital solutions are available from WDS.

Star	P (yr)	a (mas)	e	i [°]	Ω [°]	Ω [°]	τ (MJD)	WDS ID	q
GJ 195	338.	3720	0.0	65.	168.5	0.0	55197	05167+4600	5
GJ 352	18.4	630	0.29	143.	48.	285.	45663	09313–1329	3
GJ 569B	2.424	90.4	0.312	32.4	321.3	256.7	51821	14545+1606	2
GJ 661	12.9512	762	0.743	149.14	160.	99.	48373	17121+4540	2
GJ 860	44.67	2383	0.41	167.2	154.5	211.	40666	22280+5742	2

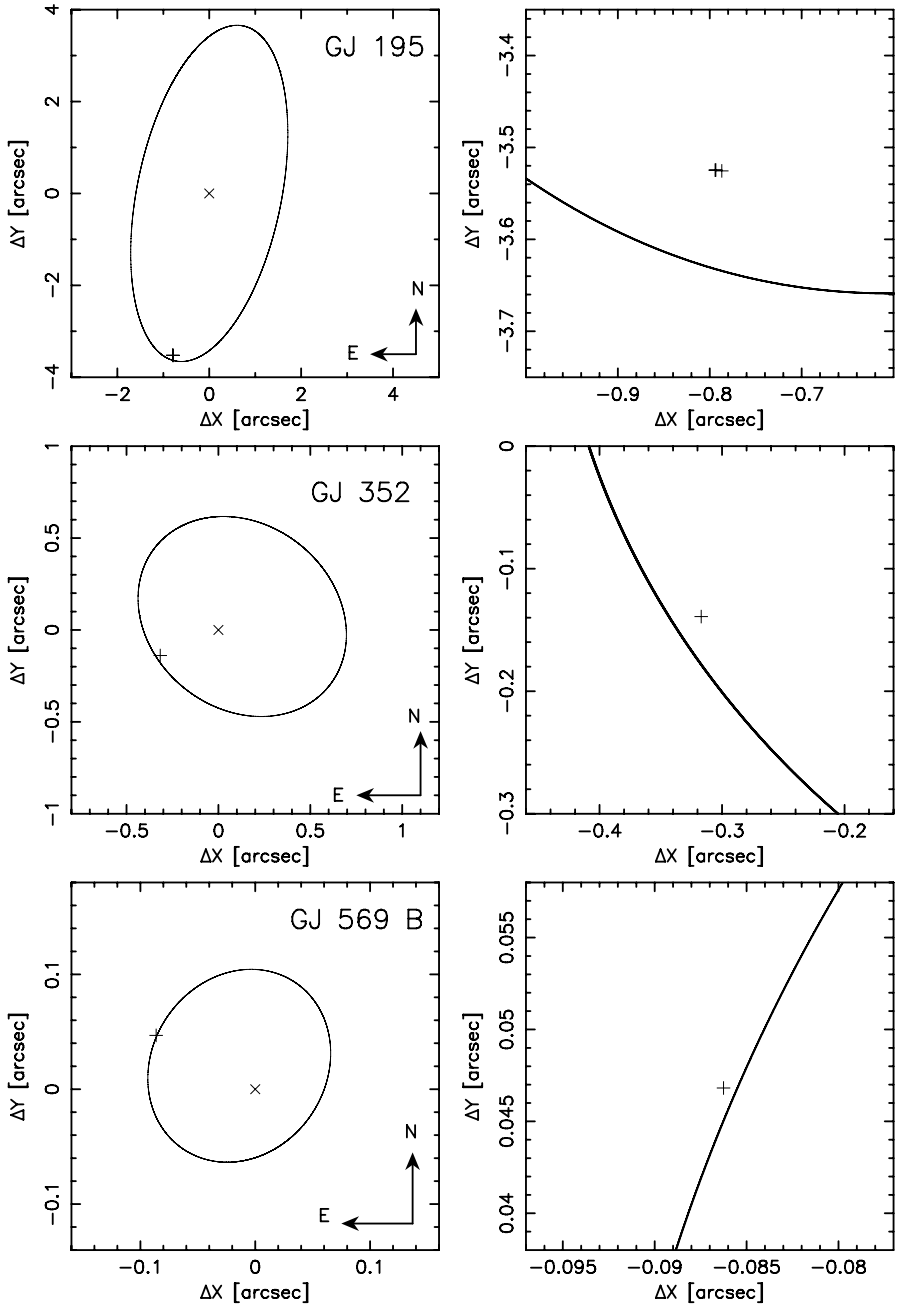

Figure 7. Relative orbits from WDS compared with our astrometry. Right panels are zoomed in on the secondary's position. The formal error bars are smaller than the symbols used. The discrepancy is probably dominated by the quality of the orbital solutions.

In Fig. 7, the comparison between the orbit and our measurements is shown. There are several possible sources of the discrepancy between our data and the orbits: (1) the quality of the orbits; (2) the uncertainty in the pixel scale; (3) an imperfect ADR correction. The level of the discrepancies ($\sim$100 mas for GJ 195 and GJ 860, $\sim$20 mas for GJ 352) seems to favour the first explanation. Also, if the cause was the ADR correction, one would expect a much higher scatter (see the next section).

5.1 Overnight and long-term astrometric precision

During one night, for most of the binaries observed with the Hale telescope we were able to go down below 500 μas in astrometric precision of ρ and in some cases below 100. As expected, the precision is better for objects for which more single images were obtained. For pairs with similar brightness of the components, the astrometric error is smaller than for pairs with a high brightness difference. This is due to the poor S/N of the faint component as well as a need not to saturate the bright one. It is imaginable that the usage of weighting might improve the precision a little.

In some cases when the stars are located on two different parts of the chip's mosaic, the astrometric errors are larger. In particular, for a very frequently observed, relatively close binary GJ 661 we achieved the highest overnight precision of 38 μas. Despite the fact that in this case the distortion correction is not perfect due to a

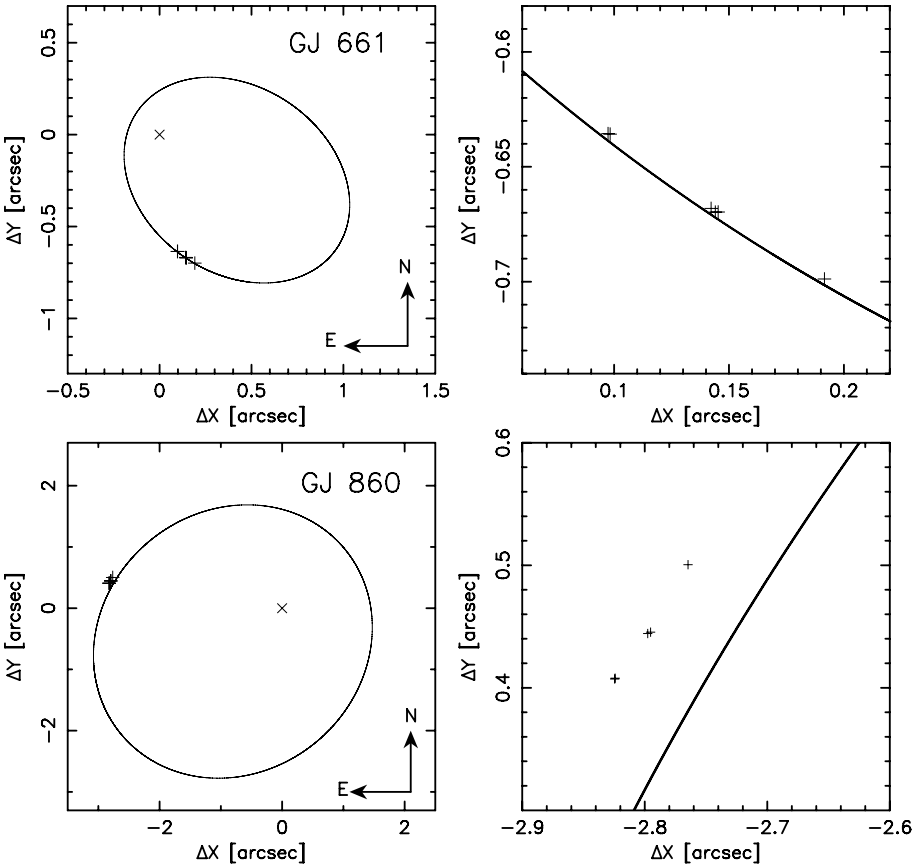

Figure 7 – *continued*

location of the binary around the centre of the chip where all four parts of the mosaic meet, Metchev (2006) suggest not to use this area because of small differences in the chip's components geometry. It seems possible that for a binary like GJ 661, one may be able to achieve a precision even below our 38 μas in one night.

We achieved a similar level of overnight precision with the Keck II/NIRC2. The main difference between the two data sets is the significantly lower number of images. It is quite surprising that with 10 frames taken with the 'narrow' camera we reached ∼120 μas precision for GJ 300. Nevertheless, one should treat this value cautiously. A low number of useful images does not allow for a particularly accurate calibration.

Three systems GJ 661, GJ 860, GJ 873 and the open cluster NGC 6871 were observed more frequently than the remaining targets. Using their measurements, we can estimate the astrometric accuracy of the Hale telescope over a 120–140 d time span. For the open cluster we take only pairs with star No. 5 which we believe is not a member of the cluster. Having five or six (for GJ 661) epochs, we can fit a second-order polynomial to the measured separations. Such a polynomial is sufficient to model the proper, parallactic and orbital motion of a close pair of stars. The fits are shown in Fig. 8. The *rms*' for all fits are collected in Table 8. Note that again the resulting *rms*' are worse for pairs with very high brightness ratios such as those for GJ 860 with the star no. 3 and GJ 873 with the star no. 1. These *rms*′ are also obviously higher than single night precisions for the corresponding pairs of stars and can be treated as an estimate for the true astrometric errors incorporating systematic effects due to an imperfect plate-scale calibration, limited knowledge of the weather conditions and long-term astrometric stability of the telescopes/cameras which could not be accounted for with our limited calibrations.

5.2 Detection limits

The astrometric signal, Θ (μas), of a planet with a semimajor axis a (au) and mass $M_{\rm P}$ (Jupiter masses) in a circular orbit around a star at a distance d (parsecs) and mass $M_{\rm S}$ (solar units) is given by (Pravdo & Shaklan 1996)

$$\Theta = 1920 \frac{a}{d} \frac{M_{\rm P}}{M_{\rm S}}. \quad (4)$$

Obviously, the same relation can be used for an S-type planet[6] in a wide binary system. Assuming that an astrometric signal above $3\sigma_\rho$ can be treated as a real one, Θ in equation (4) may be replaced by $3\sigma_\rho$ (mas) (from Table 6). After changing d (pc) to parallax π (mas) we obtain

$$a M_{\rm P}\,[\text{au } M_{\rm J}] = 1562.5 \frac{\sigma_\rho M_{\rm S}}{\pi}. \quad (5)$$

In the above $a M_{\rm P} = 4$ [au $M_{\rm J}$] means that we can detect 1 $M_{\rm J}$ (or more massive) planet in 4 au (or wider) orbit, or 2 $M_{\rm J}$ planet in 2 au orbit, etc.

[6] S-type, or satellite-type planet in binary/multiple is a planet orbiting only one of the components (Dvorak 1984).

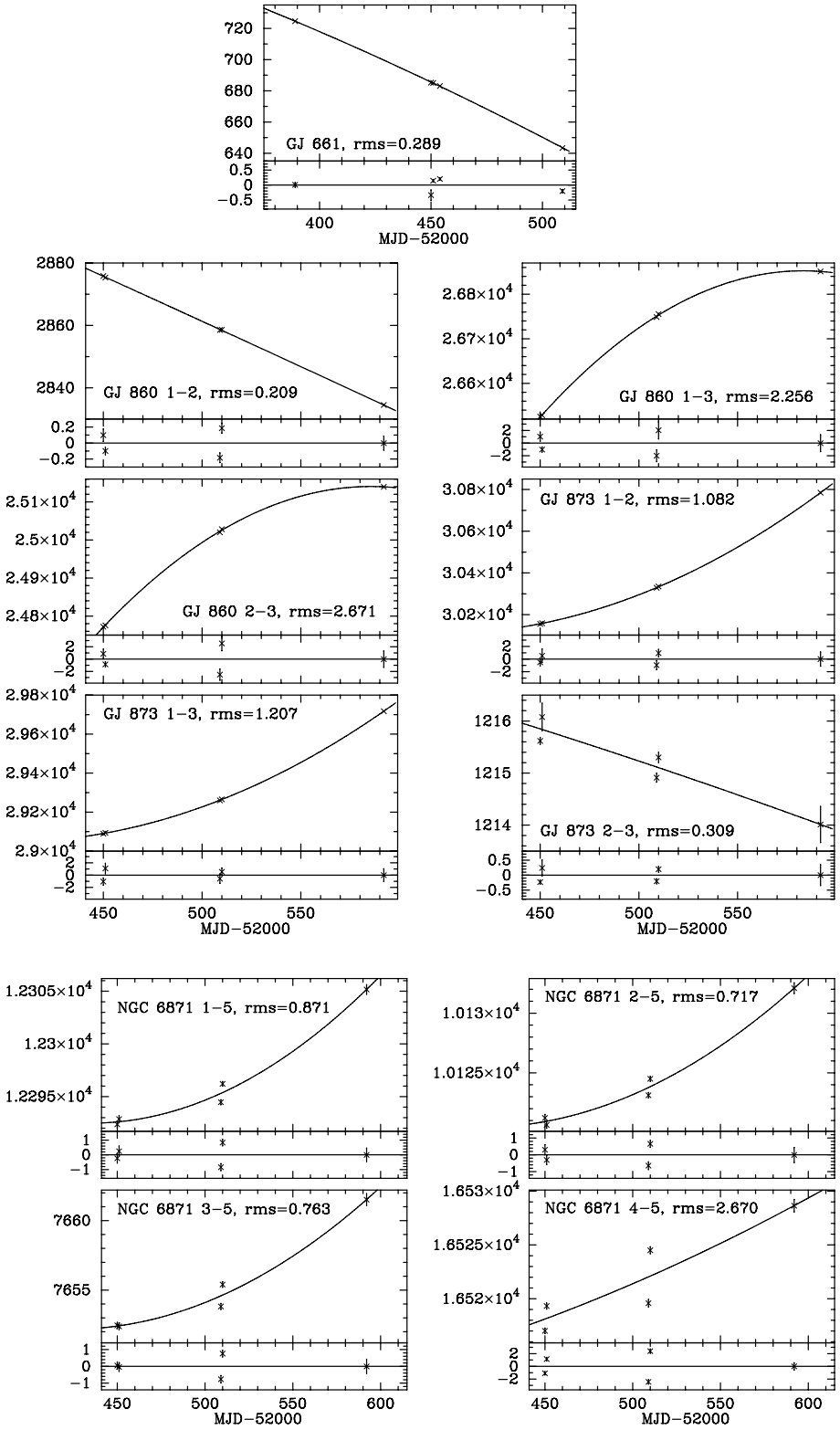

Figure 8. A second-order polynomial fits to the separations of stars from Table 8.

The detection limits for the binaries, in which at least one stellar mass is known or can be estimated, are collected in Table 9. Subscripts *I* and *II* refer to the order of stars given in the first column. As one can see, in principle, it is possible to achieve a sufficient astrometric precision to detect a massive planet or a brown dwarf with the Hale and Keck telescopes. As we have demonstrated in the previous section, currently a longer term precision is up to several times lower than the one achieved over one night. However, one can

Table 8. The *rms* of second-order polynomial fits to the measurements of ρ for the most frequently observed objects.

Pair	*rms* (mas)	No. of nights	Time span (d)
GJ 661 1–2	0.282	6	122
GJ 860 1–2	0.216	5	143
1–3	2.154		
2–3	2.595		
GJ 873 1–2	1.127	5	143
1–3	1.282		
2–3	0.309		
NGC 6871 1–5	0.872	5	143
2–5	0.717		
3–5	0.763		
4–5	2.671		

use the *rms*′ from Table 8 with equation (5) and compute long-term planetary detection limits. These long-term limits' are also listed in Table 9.

6 CONCLUSIONS

Nearby binary and multiple star systems are excellent targets for astrometric searches for extrasolar planets, thanks to their proximity and the availability of natural reference stars necessary for relative astrometry. In our study of 12 visual binaries/multiples and one open cluster with the Hale and Keck II telescopes and their adaptive optics facilities, we have demonstrated that over one night one is able to obtain an astrometric precision reaching ∼40 μas. Such a precision is sufficient to detect Jupiter mass planets around components of binary and multiple stars. However, in order to turn the precision into a long-term accuracy required to detect planets, one must be able to account for ADR and the plate-scale changes. The ADR correction requires accurate weather readings and the plate-scale changes must be carefully calibrated. In our attempt to account for both, we were able to achieve a long-term (over a 140 d time-span) accuracy ranging from 0.2 to 2.7 mas, that is several times larger than the corresponding overnight precision, but still allowing for detection of massive planets or brown dwarfs. Since we have had limited means to carry out the calibrations, it is quite possible that a higher long-term accuracy can be reached with the existing AO facilities.

ACKNOWLEDGMENTS

MK is supported by the Foundation for Polish Science through a FOCUS grant and fellowship. This work was supported by the Polish Ministry of Science and Higher Education through grants N203 005 32/0449 and 1P03D-021-29, and by NASA through grant NNG04GM62G.

This publication made use of data products from the Two-Micron All Sky Survey, which is a joint project of the University of

Table 9. $a\,M_{\rm P}$ limits.

Pair	π (mas)	M_I ($M_\odot$)	M_{II} ($M_\odot$)	σ_ρ (mas)	MJD	$a_I M_{{\rm P},I}$ [au $\cdot M_{\rm J}$]	$a_{II} M_{{\rm P},II}$ [au $\cdot M_{\rm J}$]	Ref.
GJ 195 1–2	72.0	0.53	0.19	0.31	52509	3.56	1.28	1
				0.23	52510	2.65	0.95	
				0.12	52592	1.38	0.50	
GJ 195 1–3		0.53	–	0.50	52509	8.28	–	1
				0.44	52510	5.06	–	
				0.24	52592	2.76	–	
GJ 195 1–4		0.53	–	0.54	52509	6.21	–	1
				0.47	52510	5.41	–	
				0.23	52592	2.64	–	
GJ 195 2–3		0.19	–	0.43	52509	1.77	–	1
				0.46	52510	1.90	–	
				0.24	52592	0.99	–	
GJ 195 2–4		0.19	–	0.51	52509	2.10	–	1
				0.47	52510	1.94	–	
				0.21	52592	0.87	–	
GJ 352 1–2	94.95	0.44	0.41	1.11	52389	8.04	7.49	2
GJ 458 1–2	65.29	0.40	0.37	0.40	52389	3.83	3.54	3
				0.28	52450	2.68	2.48	
				0.36	52451	3.45	3.19	
GJ 507 1–2	75.96	0.46	0.37	0.45	52389	3.70	3.43	3
				0.33	52450	3.12	2.51	
				0.36	52451	6.25	5.03	
GJ 569B 1–2	101.91	0.071	0.054	0.11	52337	0.012	0.009	4
GJ 661 1–2	158.17	0.379	0.34	0.079	52389	0.30	0.29	5
				0.170	52450	0.63	0.62	
				0.044	52451	0.17	0.16	
				0.038	52454	0.16	0.15	
				0.058	52509	0.22	0.21	
				0.041	52510	0.17	0.16	
				0.282	Total	1.05	1.03	

Table 9 – *continued*

Pair	π (mas)	M_I ($M_\odot$)	M_{II} ($M_\odot$)	σ_ρ (mas)	MJD	$a_I M_{P,I}$ [au $\cdot M_J$]	$a_{II} M_{P,II}$ [au $\cdot M_J$]	Ref.
GJ 767 1–2	74.9	0.44	0.4	0.17	52509	1.56	1.42	3
				0.12	52510	1.10	1.00	
				0.09	52592	0.83	0.75	
GJ 767 1–3		0.44	–	0.52	52509	4.77	–	3
				0.28	52510	2.57	–	
				0.39	52592	3.58	–	
GJ 767 2-3		0.4	–	0.43	52509	3.59	–	3
				0.22	52510	1.83	–	
				0.35	52592	2.92	–	
GJ 860 1–2	249.53	0.34	0.2711	0.078	52450	0.17	0.13	5
				0.048	52451	0.10	0.09	
				0.061	52509	0.13	0.10	
				0.061	52510	0.13	0.10	
				0.087	52592	0.18	0.15	
				0.216	Total	0.45	0.37	
GJ 860 1–3		0.34	–	0.73	52450	1.55	–	5
				0.41	52451	0.86	–	
				0.94	52509	2.01	–	
				1.37	52510	2.95	–	
				1.34	52592	2.86	–	
				2.154	Total	4.60	–	
GJ 860 2–3		0.2711	–	0.75	52450	1.28	–	5
				0.42	52451	0.71	–	
				0.91	52509	1.29	–	
				1.19	52510	2.02	–	
				1.33	52592	2.54	–	
				2.595	Total	4.96	–	
GJ 873 1–2		0.36	–	0.57	52450	1.62	–	3
				1.07	52451	3.04	–	
				0.73	52509	2.07	–	
				0.60	52510	1.71	–	
				1.12	52592	3.20	–	
				1.127	Total	3.29	–	
GJ 873 1–3	198.07	0.36	–	0.58	52450	1.65	–	3
				0.85	52451	2.41	–	
				0.76	52509	2.16	–	
				0.61	52510	1.73	–	
				1.03	52592	2.93	–	
				1.282	Total	3.65	–	
GJ 9071 1–2	72	0.53	0.49	0.20	52509	2.22	2.05	3
				0.26	52510	2.89	2.67	
				0.24	52592	2.66	2.46	

References: (1) Fischer & Marcy (1992); (2) Söderhjelm (1999); (3) Harmanec (1988); (4) Zapatero Osorio et al. (2004); (5) Delfosse et al. (2000).
Note: If *MJD* is 'Total', the limit refers to the *rms* of the fit given in Table 8 – an estimate of a long-term astrometric precision for a given pair of stars.

Massachusetts and the Infrared Processing and Analysis centre California Institute of Technology, funded by the NASA and the National Science Foundation.

REFERENCES

Al-Shukri A. M., McAlister H. A., Hartkopf W. I., Hutter D. J., Franz O. G., 1996, AJ, 111, 393
Barstow M. A., Bond H. E., Burleigh M. R., Holberg J. B., 2001, MNRAS, 322, 891
Benedict G. F. et al., 2002, ApJ, 581, L115
Benedict G. F. et al., 2006, AJ, 132, 2206
Cameron P. B., Britton M. C., Kulkarni S. R., 2009, AJ, 137, 83
Cutri R. M. et al., 2003, The IRSA 2MASS All-Sky Point Source Catalog, NASA/IPAC Infrared Science Archive. http://irsa.ipac.caltech.edu/applications/Gator/
Delfosse X., Forveille T., Ségransan D., Beuzit J.-L., Udry S., Perrier C., Mayor M., 2000, A&A, 364, 217
Dommanget J., Nys O., 2002, Observations et Travaux, 54, 5
Dvorak R., 1984, Celest. Mech., 34, 369
Eggenberger A., Udry S., Chauvin G., Beuzit J.-L., Lagrange A.-M., Ségransan D., Mayor M., 2007, A&A, 474, 273
Eisenhauer F. et al., 2008, IAUS, 248, 100
Fischer D. A., Marcy G. W., 1992, ApJ, 396, 198
Han I., Black D. C., Gatewood G., 2001, ApJ, 548, L57
Harmanec P., 1988, Bull. Astron. Inst. Czech., 39, 329

Hayward T. L., Brandl B., Pirger B., Blacken C., Gull G. E., Schoenwald J., Houck J. R., 2001, PASP, 113, 105
Heintz W. D., 1974, ApJ, 195, 411
Hełminiak K. G., 2009, New Astron., 14, 521
Holman M., Weigert P. A., 1999, AJ, 117, 621
Henry T. J., Jao W.-C., Subasavage J. P., Beaulieu T. D., Ianna P. A., Costa E., Méndez R. A., 2006, AJ, 132, 2360
Jenkins L. F., 1952, General Catalogue of Trigonometric Stellar Parallaxes. Yale Univ. Obs., New Haven
Lane B. F., Muterspaugh M. W., 2004, ApJ, 601, 1129
Launhardt R. et al., 2008, IAUS, 248, 417
Law N. M., Hodgkin S. T., McKay C. D., 2008, MNRAS, 384, 150
Lissauer J. J., Quintana E. V., Chambers J. E., Duncan M. J., Adams F. C., 2004, Rev. Mex. Astron. Astrofis. Conf. Ser., 22, 99
Metchev S. A., 2006, PhD thesis, California Institute of Technology
Metchev S. A., Hillenbrand L. A., 2004, ApJ, 617, 1330
Metchev S. A., Eisner J. A., Hillenbrand L. A., Wolf S., 2005, ApJ, 622, 451
Mugrauer M., Neuhäuser R., 2009, A&A, 494, 373
Muterspaugh M. W., Lane B. F., Konacki M., Burke B. F., Colavita M. M., Kulkarni S. R., Shao M., 2005, AJ, 130, 2866
Muterspaugh M. W., Konacki M., Lane B. F., Pfahl E., 2007, preprint (arXiv:0705.3072v1)
Nelson A. F., 2000, ApJ, 537, L65
Neuhäuser R., Seifhart A., Röll T., Bedalov A., Murgrauer M., 2006, in Hartkopf W. I., Guinan E. F., Harmanec P., eds, IAU Symp. 240, Binary Stars as Critical Tools & Tests in Contemporary Astrophysics. Cambridge Univ. Press, Cambridge, p. 261
Oppenheimer B. R., Golimowski D. A., Kulkarni S. R., Matthews K., Nakajima T., Creech-Eakman M., Durrance S. T., 2001, AJ, 121, 2189
Perryman M. A. C., 2005, in Seidelman P. K., Monet A. K. B., eds, ASP Conf. Ser. Vol. 338, Astrometry in the Age of the Next Generation of Large Telescopes. Astron. Soc. Pac., San Francisco, p. 3
Perryman M. A. C. et al., 1997, A&A, 323, L49
Pravdo S. H., Shaklan S. B., 1996, ApJ, 465, 264
Pravdo S. H., Shaklan S. B., 2009, ApJ, 700, 623
Raghavan D., Henry T. J., Mason B. D., Subasavage J. P., Jao W.-C., Beaulieu T. D., Hambly N. C., 2006, ApJ, 643, 523
Reid I. N. et al., 2004, AJ, 128, 463
Roe H. G., 2002, PASP, 114, 450
Roeser S., Bastian U., 1988, A&AS, 74, 449
Röll T., Seifhart S., Neuhäuser R., 2008, in Sun Y.-S., Ferraz-Mello S., Zhou J.-L., eds, IAU Symp. 249, Exoplanets: Detection, Formation & Dynamics. Cambridge Univ. Press, Cambridge, p. 57
Sahlmann J., Abuter R., Ménardi S., Vasisht G., 2008, in Jin W., Platais I., Perryman M. A. C., eds, IAU Symp. 248, A Giant Step: From Milli- to Micro-Arcsecond Astrometry. Cambridge Univ. Press, Cambridge, p. 124
Simon M., Bender C., Prato L., 2006, ApJ, 644, 1183
Simons D. A., Henry T. J., Kirkpatrick J. D., 1996, AJ, 112, 2238
Söderhjelm S., 1999, A&A, 341, 121
Stetson P. B., 1987, PASP, 99, 191
Thompson D., Egani E., Sawicki M., 2001, NIRC-2. The Keck New-Infrared AO Camera. Pre-ship testing, California Institute of Technology, Pasadena
Unwin S. C. et al., 2008, PASP, 120, 38
Zapatero Osorio M., Lane B. F., Pavlenko Y., Martín E. L., Britton M., Kulkarni S. R., 2004, ApJ, 615, 958

This paper has been typeset from a TEX/LATEX file prepared by the author.